

Observations of water vapor by ground-based microwave radiometers and Raman lidar

Yong Han, J. B. Snider, and E. R. Westwater

NOAA Environmental Research Laboratory, Boulder, Colorado

S. H. Melfi

Laboratory for Atmospheres, NASA Goddard Space Flight Center, Greenbelt, Maryland

R. A. Ferrare

Hughes-STX Corporation, Lanham, Maryland

Abstract. In November to December 1991, a substantial number of remote sensors and in situ instruments were operated together in Coffeyville, Kansas, during the climate experiment FIRE II. Included in the suite of instruments were (1) the NOAA Environmental Technology Laboratory (ETL) three-channel microwave radiometer, (2) the NASA GSFC Raman lidar, (3) ETL radio acoustic sounding system (RASS), and (4) frequent, research-quality radiosondes. The Raman lidar operated only at night and the focus of this portion of the experiment concentrated on clear conditions. The lidar data, together with frequent radiosondes and measurements of temperature profiles (every 15 min) by RASS allowed profiles of temperature and absolute humidity to be estimated every minute. We compared 2-min measurements of brightness temperature (T_b) with calculations of T_b that were based on the Liebe and Layton (1987) and Liebe et al. (1993) microwave propagation models, as well as the Waters (1976) model. The comparisons showed the best agreement at 20.6 GHz with the Waters model, with the Liebe et al. (1993) model being best at 31.65 GHz. The results at 90 GHz gave about equal success with the Liebe and Layton (1987) and Liebe et al. (1993) models. Comparisons of precipitable water vapor derived independently from the two instruments also showed excellent agreement, even for averages as short as 2 min. The rms difference between Raman and radiometric determinations of precipitable water vapor was 0.03 cm which is roughly 2%. The experiments clearly demonstrate the potential of simultaneous operation of radiometers and Raman lidars for fundamental physical studies of water vapor.

1. Introduction

In radiometric remote sensing of the atmosphere the ability to calculate radiances from underlying state variables is fundamental. For example, to infer temperature and water vapor profiles from satellites, one must determine cloud-free regions and then calculate clear-sky radiance emerging from the top of the Earth's atmosphere from the underlying profiles of temperature and water vapor [Rao et al., 1990]. Similar needs occur when measuring precipitable water vapor from ground-based radiometers [Westwater, 1993]. Traditionally, such "forward model" calculations have coupled radiosonde observations of the state variables with detailed absorption and radiative transfer models to compare with radiance observations [Fleming et al., 1991; England et al., 1993]. However, for a variety of reasons, radiosonde moisture measurements are not always satisfactory, especially during low-humidity conditions [Westwater et al., 1989; Melfi et al., 1989; Garand et al., 1992; Elliott and Gaffen, 1991], or when there are large horizontal or temporal

gradients in the humidity structure. A recent alternative to radiosonde moisture measurements in Raman lidar [Melfi and Whiteman, 1985; Melfi et al., 1989; England et al., 1992]. In the work of England et al. [1992] a comparison was made of water vapor measurements by a Goddard Space Flight Center (GSFC) Raman water vapor lidar and a microwave radiometer during the Atmospheric Moisture Inter-comparison Study (ATMIS). Here, an upgraded Raman instrument (see section 2.2) was used.

In November to December 1991 a substantial number of remote sensors and in situ instruments were operated together in Coffeyville, Kansas, during the climate experiment FIRE II. Included in the suite of instruments were (1) the NOAA Environmental Technology Laboratory (ETL) three-channel microwave radiometer, (2) the NASA GSFC Raman lidar, (3) ETL radio acoustic sounding system (RASS) [May et al., 1988], and (4) frequent, research-quality radiosondes. The Raman lidar operated only at night and the focus of this portion of the experiment concentrated on clear conditions. In this paper we present results of simultaneous microwave radiometer measurements with collocated Raman lidar measurements of water vapor. Information on temperature profiles was also obtained from composite data from radiosondes and RASS.

This paper is not subject to U.S. copyright. Published in 1994 by the American Geophysical Union.

Paper number 94JD01487.

2. Description of Equipment

2.1. NOAA Transportable Three-Channel Microwave Radiometer

The NOAA transportable microwave radiometer is a three-frequency system whose primary product are the column abundances of liquid water in clouds and water vapor in the atmosphere. The system is completely passive and detects the natural emission of microwave energy by liquid water and water vapor. Measured quantities, after a calibration procedure that takes into account internal radiometer temperatures and voltages, are expressed as brightness temperatures. From the brightness temperatures, a simple retrieval algorithm is used to derive the path integral of liquid water and water vapor in the direction observed by the instrument.

The system contains three independent microwave radiometers: the first operates at 20.6 GHz (wavelength = 1.46 cm) and is sensitive primarily to water vapor; the second operates at 31.65 GHz (wavelength = 0.948 cm) and is sensitive primarily to liquid water; the third operates at 90.0 GHz (wavelength = 0.333 cm) and is sensitive to both vapor and liquid. However, the 90-GHz channel is approximately 6 times more sensitive to liquid water than the 31.65-GHz channel; thus the third frequency increases the sensitivity of the instrument to small amounts of cloud liquid. A more complete description of the system is given by *Westwater et al.* [1990]. A basic feature of the instrument is that all three channels have the same beam width of 2.5°. Although the instrument is scannable in both elevation and zenith, our observations here were in the zenith direction only.

The brightness temperatures of the three channels were calibrated by the so-called "tipping curve" calibration procedure [Decker and Schroeder, 1991], a technique which is completely independent of either radiosondes or Raman lidar. Since the absolute calibration of the instrument is fundamental to the studies conducted here, we will outline the technique that we use. With a switching circuit, each channel sequentially views (1) a temperature reference blackbody "load" whose temperature T_r is measured, (2) a hot blackbody whose temperature T_h is also measured, and (3) the apparent brightness temperature of the atmosphere T_b . The noise powers from these loads are mixed with the signal from a local oscillator, amplified, and detected by a square law detector whose DC output voltage is proportional to its input power. These three voltages are v_r , v_h , and v_m , respectively. The circuit was constructed to have several elements at the temperature T_r . The gain of the system is measured approximately every 0.3 s by measuring the voltages from the hot and reference loads. However, we must also correct for small changes in power due to passage of the input atmospheric brightness temperature through a mylar window, through a small microwave horn, and through a short portion of waveguide. We use a single parameter, or loss factor X_1 , to correct for these changes. In terms of this factor our equation to derive atmospheric brightness temperature from the measured voltages and internal temperatures is

$$T_b = X_1 \left[\frac{v_m - v_r}{v_h - v_r} (T_h - T_r) \right] + X_1 (T_r - T_w) + T_w \quad (1)$$

At frequencies where the atmospheric absorption is small, the radiometer calibration constant X_1 can be determined by

the tipping curve method. This method requires a set of radiometer brightness temperature measurements at several different elevation angles when the atmosphere is horizontally stratified. The horizontal stratification assumption typically requires clear atmospheric conditions. The elevation angles are chosen to represent a range of air masses, where air mass is approximately equal to the cosecant of the elevation angle; the cosecant law neglects the effects of Earth curvature and refraction.

To establish a linear relationship between the radiometer measurements and the air mass, the brightness temperatures T_b measured at each elevation angle are converted to total absorption τ (Np), which is linear with air mass. The Rayleigh-Jeans approximation to the Planck function allows the simple conversion from T_b to absorption

$$\tau = \ln \frac{T_{mr} - T_{bg}}{T_{mr} - T_b} \quad (2)$$

where T_{mr} is mean radiating temperature (K) and T_{bg} is the cosmic background radiation (K). Because the value chosen for T_{mr} is not critical for clear conditions at these frequencies, we use a monthly value appropriate to the radiometer location. We use 2.75 K for T_{bg} [Wilkinson, 1986]. Since no absorption can occur at air mass = 0, measurements of τ at air mass values of 1, 2, and 3 are extrapolated to zero air mass. If $\tau(0) \neq 0$, the X_1 is adjusted to bring it to zero. In practice, we use a least squares procedure to determine X_1 , from T_b measurements at several zenith and azimuth angles. Subject to the assumption that the radiometer equation (1) is correct, this procedure leads to an absolute calibration in terms of X_1 .

For the Coffeyville, Kansas, experiment, we performed 11 separate tip calibrations throughout the two months of the 1991 experiment. Based on the variations in X_1 over these calibrations, we give the 99% confidence limits for the absolute accuracy of our measurements at 20.6, 31.65, and 90.0 GHz as (± 0.5 , ± 0.9 , ± 1.4 K). The corresponding rms values for the sensitivities, at our 2-min averaging time, are (0.03, 0.02, 0.11 K).

2.2. Raman Lidar

For the FIRE II results reported here, a new NASA GSFC Raman water vapor lidar system was deployed. This lidar, described by *Whiteman et al.* [1992a] and *Ferrare et al.* [1992], incorporated many new features and was significantly improved over the previous system used during ATMIS described by *Melfi and Whiteman* [1985], *Melfi et al.* [1989], and *Whiteman et al.* [1992b]. The characteristics of this new lidar as operated during the FIRE II experiment will be discussed here briefly. The system uses a XeF laser to transmit light at 351 nm. A telescope collects the backscattered energy from a variety of sources and wavelengths, including aerosol and molecular backscattered light at the laser wavelengths as well as Raman-scattered light from water vapor (403 nm), nitrogen (383 nm), and oxygen (372 nm) molecules. Beam splitters are used to separate the return signals into low- and high-sensitivity channels; these two channels are employed for each wavelength to measure signals throughout the troposphere. The low-channel data are used from near the surface to an altitude of about 4 km; between 4 and 5 km the high-channel data gradually replace the low-channel data so that after about 5 km the high-

channel data are used exclusively. Photomultiplier tubes detect the backscattered radiation in all channels and provide output signals to photon counters. In normal operation, data from more than 23,000 shots are recorded as 1-min profiles with a range resolution of 75 m.

Profiles of water vapor mixing ratio are computed from the ratio of the Raman water vapor to Raman nitrogen return signals [England *et al.*, 1992]. A small correction (<7% for altitudes below 12 km) is applied to account for the differential atmospheric transmission between these two Raman wavelengths. Although this correction generally can be computed with sufficient accuracy using density and aerosol profiles from standard atmospheric models, the present method uses the density profiles computed from coincident and collocated radiosondes and the aerosol extinction profiles measured by the Raman lidar.

The water vapor mixing ratio is proportional to the ratio of Raman scattering by water vapor to Raman scattering by nitrogen. The lidar water vapor mixing ratio profiles are calibrated using a weighted least squares regression of the lidar ratios to the water vapor mixing ratios measured by coincident radiosondes launches at the lidar site. Radiosonde data below 30% relative humidity are not used because of potential and unreliable radiosonde moisture measurements in dry conditions [Wade and Wolf, 1989; Garand *et al.*, 1992]. During the 3-week FIRE II experiment period, there were 41 radiosonde humidity profiles used for calibration. Of these 41 radiosonde profiles, 24 were made using carbon hygistor elements, while 17 were made using capacitive elements. Initial results from these and other comparisons indicate that the lidar water vapor mixing ratio calibration constant derived using the radiosonde capacitive humidity sensor measurements is systematically 7–10% lower than that using the carbon hygistor humidity measurements. Since it is not clear which (if either) radiosonde humidity sensor provides the more accurate humidity measurement, the lidar calibration constant was found using data from all 41 comparisons, so that the lidar water vapor mixing ratios lie approximately halfway between those measured by the two radiosonde sensors.

The random error associated with the lidar water vapor mixing ratio profiles is computed using Poisson statistics (i.e., the noise is given by the square root of the total number of photon counts). Both Raman water vapor and nitrogen channels contribute to this error which increases with altitude. For a 1-min profile the random error is less than 10% for altitudes below 7.5–8.5 km. This maximum altitude depends on averaging time, vertical resolution, ambient water vapor amounts, background skylight, and aerosol attenuation. By averaging for longer periods of time, and/or by reducing the vertical resolution, profiles above 8.5 km can be obtained [Soden *et al.*, 1994]. Clouds rapidly attenuate the laser beam so that water vapor retrievals are generally limited to altitudes below cloud base. Since the lidar also measures scattering by aerosols and clouds, these cloud base altitudes are easily identified from the lidar data.

2.3. Radio Acoustic Sounding System (RASS)

The ETL RASS profiler operated at 404.37 MHz and usually reported averaged measurements every 15 min. The major characteristics of this transportable instrument, which usually operates in Erie, Colorado, are outlined by Martner *et al.* [1993]. For our purposes the relevant system param-

eters are the range resolution of 150 m, the lowest range gate of 350 m, and the maximum upper range, which varied from 1 to 2 km. During the FIRE II experiment, the upper range was unusually limited due to problems with winds and radio interference.

3. Comparison of Brightness Temperature Measurements and Calculations

Previously, comparisons of measured and calculated brightness temperatures have been reported [Westwater *et al.*, 1990; England *et al.*, 1993]. In the earlier work, clear-sky measurements of zenith radiance at 20.6, 31.65, and 90.0 GHz were compared with calculations based on the absorption models of Waters [1976] and of Liebe and Layton [1987]. Radiosonde soundings of temperature T , relative humidity RH, and pressure P provided the input profiles for the radiative transfer models. Data from both radiometers and radiosondes were carefully screened to eliminate spurious points. These data indicated that modifications of absorption parameters were necessary to produce agreement between measurements and calculations.

Recently, both water vapor [Liebe *et al.*, 1993] and oxygen [Liebe *et al.*, 1992] absorption models have been updated. In these recent models the values of parameters describing the 22.235-GHz water vapor line, the 60-GHz oxygen band, and the water vapor continuum have been changed from those reported by Liebe and Layton [1987] and by Liebe [1989]. In this section we compare measurements of brightness temperature with calculations based on Waters [1976] and both the previous (1987) and the more recent absorption models of Liebe *et al.* For convenience we will refer to the models as RTE76 (Waters [1976] for H₂O, Rosenkranz [1988] for O₂), RTE87 (Liebe and Layton [1987] for H₂O, Rosenkranz [1988] for O₂), and RTE93 (Liebe *et al.* [1993] for H₂O, Liebe *et al.* [1992] for O₂). Here, in contrast to previous work that was based on radiosondes, we use 2-min measurements of water vapor profiles provided by the Raman lidar, together with temperature profiles provided by RASS merged with radiosondes.

Although remote sensors provided the bulk of the profile data, data in the first ≈ 300 m above ground level were derived by other means. The profiles below the lowest range gates of the Raman lidar (185 m) and the RASS (350 m) were estimated by linear interpolation using ETL surface meteorological measurements. Typical disagreements between ETL and radiosonde surface measurements of absolute humidity were about 0.5 g/m³. The temperature data were collected from a variety of instruments and then interpolated onto a uniform time/height grid. Radiosonde measurements were often many hours apart but were sometimes as close as minutes. The ETL RASS profiler usually reported averaged measurements every 15 min. The ETL 2-min surface meteorological data were averaged to provide data on the same temporal interval as RASS, i.e., every 15 min. Temperatures from the surface station and rawinsondes were converted to virtual temperature (which is the basic quantity measured by RASS). To derive brightness temperatures on the 2-min temporal scale, the temperature profiles were interpolated to the Raman spatial and temporal grid. There were a total number of 2506 coincident radiometric and Raman lidar measurements available when there were clear-sky conditions during 10 nights of the experiment.

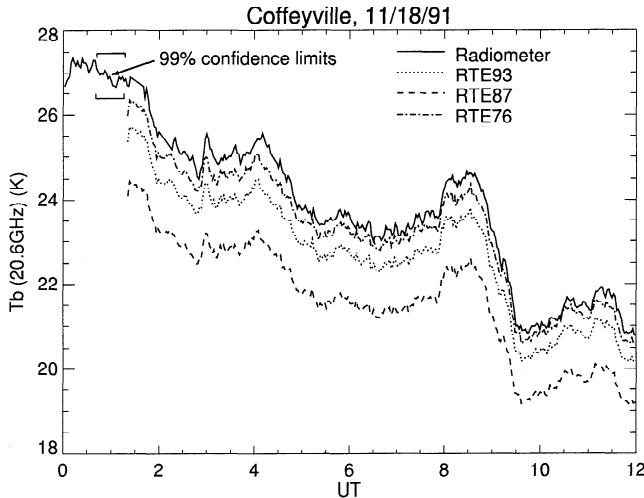


Figure 1. Time series of measured and modeled brightness temperatures at 20.6 GHz. Water vapor and temperature profiles taken from the Raman lidar and the radio acoustic sounding system are used for the model calculations.

In the original data set provided to us, there were several periods in which the Raman lidar indicated clouds; these data were eliminated. There were also some profiles for which there were isolated points (these were usually at altitudes above 5 km) where the mixing ratio was negative. For these points, positive mixing ratio values were within the random errors of the data. If the total number of such points was small (≈ 5), the negative points were deleted but the rest of the profile was used in the radiative transfer equation (RTE) calculations. Data from one complete night were deleted, even though the conditions were clear, because the Raman data were adversely affected by a low-lying layer of hygroscopic aerosols and fog. The excellent stability of the radiometer was instrumental in identifying these spurious data.

Calculations of brightness temperatures from height pro-

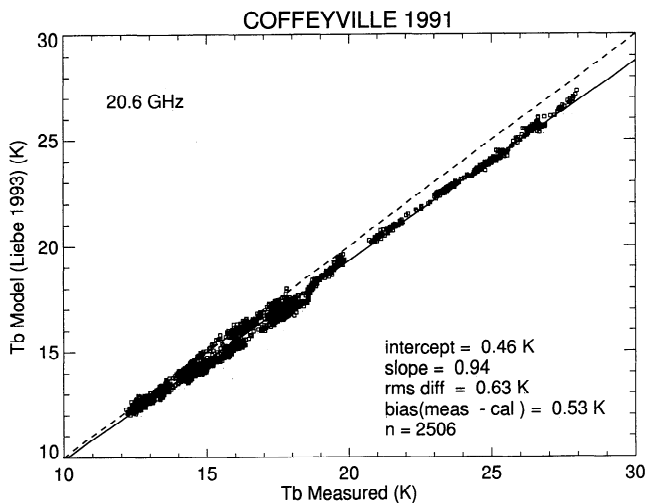


Figure 2. Comparison of measured and calculated brightness temperatures at 20.6 GHz, using absorption models RTE93. See text for details of absorption model. Dashed line is 45°, and solid line is regression.

Table 1. Comparison of Measured and Calculated Brightness Temperature at 20.6 GHz

	rms Difference K	Bias, K (Meas-Cal)	Slope	Intercept K
RTE76	0.40	0.27	0.99	-0.10
RTE87	1.48	1.41	0.90	0.28
RTE93	0.63	0.53	0.94	0.46

$N = 2506$. Meas, measured; cal, calculated.

files of temperature, water vapor, and pressure, require numerical evaluation of the RTE

$$I_\nu(T_{b,\nu}) = B_\nu(T_{bg}) \exp(-\tau)$$

$$+ \int_0^\infty B_\nu(T) \alpha_\nu \exp\left(-\int_0^h \alpha_\nu dh'\right) dh \quad (3)$$

where $T_{b,\nu}$ is brightness temperature (K) at frequency ν ; $I_\nu(T_{b,\nu})$ is radiance ($\text{W m}^{-2} \text{sr}^{-1} \text{GHz}^{-1}$); h is height in km; $T = T(h)$ is temperature at height h ; $B_\nu(T)$ is the Planck function ($\text{W m}^{-2} \text{sr}^{-1} \text{GHz}^{-1}$); and $\alpha_\nu = \alpha_\nu(h)$ is absorption coefficient (km^{-1}). The method that ETL uses in the numerical evaluation of (3), using profiles of temperature, absolute humidity, pressure, and (modeled) cloud liquid density, is given in detail by *Schroeder and Westwater* [1991]. This program also extrapolates input profiles above their last point to a pressure of 0.1 mbar using a regression method.

In Figure 1 we show typical results of comparing measured and calculated brightness temperatures for a 12-hour time period at the frequency of 20.6 GHz. It is clearly evident that there is an overall offset between measurements and calculations using RTE76, RTE87, and RTE93. However, it is encouraging that excellent correlation between measurements is obtained on the finest timescale allowed, 2 min. It is also evident that at 20.6 the RTE76 model gives almost exact agreement with measurements. We also show on the figure our estimates of the absolute accuracy at each frequency.

We supplement the results shown in Figure 1 by a statistical analysis carried out over the entire data set of clear and quality-controlled measurements. As an example, we present in Figure 2 a representative scatterplot of measured versus calculated values using RTE93 at 20.6 GHz. In addition, we present in Tables 1, 2, and 3 a summary of our linear regression results. These statistical results show the 20.6-GHz results are better with RTE76, the 31.65-GHz results are better with RTE93, and the 90-GHz results show no improvement using the RTE87 over the RTE93 model. The latter results are consistent with those of *Westwater et*

Table 2. Comparison of Measured and Calculated Brightness Temperature at 31.65 GHz

	rms Difference K	Bias, K (Meas-Cal)	Slope	Intercept K
RTE76	1.30	1.27	0.88	0.53
RTE87	1.96	1.93	0.83	0.70
RTE93	0.76	0.73	0.94	0.23

$N = 2506$.

Table 3. Comparison of Measured and Calculated Brightness Temperature at 90.0 GHz

	rms Difference K	Bias, K (Meas-Cal)	Slope	Intercept K
RTE76	7.66	-7.38	1.27	-2.36
RTE87	1.95	1.77	1.00	-1.75
RTE93	1.48	-0.04	1.18	-6.42

$N = 2506$.

al. [1990] which showed poor agreement of Waters' equations at 90.0 GHz.

The recent changes to the Liebe model RTE93 produce better agreement at 20.6 and 31.65 GHz than previous models used in RTE87. This better agreement results from improvements in the line parameters associated with the 22.235-GHz water vapor line. The rather mixed results at 90 GHz indicate that the water vapor continuum may not be so well modeled. Certainly, measurements in more humid environments would be useful in addressing these modeling questions.

4. Comparison of Precipitable Water Vapor Retrievals

Precipitable water vapor can be derived directly from the Raman lidar data, given a suitable dry air density profile, and from the radiometer data, by means of a retrieval algorithm. The radiometric retrieval algorithm that we used was the linear statistical method [Westwater, 1993], conditioned on clear-sky conditions; all three channels were used in the retrievals. In addition, we removed radiometric-RTE model offsets by adjusting the radiometer brightness temperature data to be consistent with the RTE93 calculations, using rawinsonde data as ground-truth profile data. Since our procedure differs in detail from the previous ones used by ETL, we will outline the significant details.

The total amount of water vapor in a vertical column through the atmosphere per unit cross section, the precipitable water vapor V , is given by

$$V = \int_0^{\infty} \rho_v(h) dh, \quad (4)$$

where ρ_v is density of water vapor (g m^{-3}). Since the density of liquid water is approximately 1 g/cm^3 , the units of V in g/cm^2 or in centimeters are practically interchangeable. From polar regions to the tropics, V can vary from 0.1 mm to 75 mm.

During clear conditions, V can be measured from a single emission measurement. However, during cloudy conditions,

Table 4. Regression Coefficients Between Measured and Calculated Brightness Temperature

Frequency, GHz	a , K	b
20.6	0.600	0.950
31.65	-0.017	0.965
90.0	-5.137	1.156

$$\hat{T}_{\text{cal}} = a + b * T_{b,\text{meas}} \quad 109 \text{ radiosondes.}$$

Table 5. Covariance Matrix Between Adjusted Measured and Calculated Brightness Temperature

	GHz		
	20.6	31.65	90.0
20.6	0.771	0.387	1.883
31.65	0.387	0.226	0.964
90.0	1.883	0.964	5.060

Adjustment factors were based on RTE93.

cloud liquid emits microwave energy, so that its effect must be taken into account. We designate integrated cloud liquid by L , and methods of determining both V and L are discussed by Westwater [1993]. A large body of experimental evidence now exists showing that with at least two well-chosen frequencies, both L and V can be measured simultaneously.

Our method of deriving V was conditioned on $L = 0$, which was known from the Raman lidar, and differs slightly from the usual ETL methods [Westwater, 1993]. We first derived total absorption τ (opacity) from the measured T_b using (2). Rather than using a climatological value for T_{mr} , we estimated it for each 2-min data point from a linear regression analysis. The regression coefficients were derived from an a priori ensemble of radiosondes from Oklahoma City, Oklahoma, the closest NWS radiosonde station to Coffeyville. We used the same a priori ensemble to derive V , using values of τ at the three frequencies. This equation is given by

$$\hat{V} = \langle V \rangle + S_{V\tau} S_{\tau}^{-1} (\tau - \langle \tau \rangle) \quad (5)$$

where τ is the column vector of τ_i , $i = 1, 2, 3$; $\langle V \rangle$, $\langle \tau \rangle$ is ensemble-averaged values of V , τ ; $S_{V\tau}$ is 1×3 covariance matrix between V and τ ; S_{τ} is 3×3 covariance matrix of τ ; and \hat{V} is estimated value of V .

The covariance matrices were determined from the Oklahoma City a priori ensemble using brightness temperatures calculated using RTE93. Our procedure also requires knowledge of the covariance matrix of experimental errors S_{ϵ} (in T_b). To determine this matrix as well as to convert the measured brightness temperatures into values consistent with the RTE93 software, we used a regression analysis between values of T_b calculated from radiosondes and measured values. A total of 109 radiosondes were used in this determination. The matrix S_{ϵ} was calculated by

$$S_{\epsilon} = \langle (T_{b,\text{meas}} - T_{b,\text{calc}})(T_{b,\text{meas}} - T_{b,\text{calc}})^T \rangle \quad (6)$$

where the expectation value (in angle brackets) was carried out over the joint ensemble of radiosondes and brightness temperature measurements. The adjustment coefficients and the covariance matrix are given in Tables 4 and 5. Note the close agreement between the adjustment coefficients calculated from the radiosondes and the values given in Tables 1–3 for the Raman-radiometer comparisons.

Typical V comparisons are shown in Figure 3, where Raman, microwave, and radiosonde measurements are shown. As is evident, there is excellent correlation on short timescales between Raman and microwave data, and due to the radiometric offset adjustments, there is only a small bias in V . As shown, there is also good agreement with the

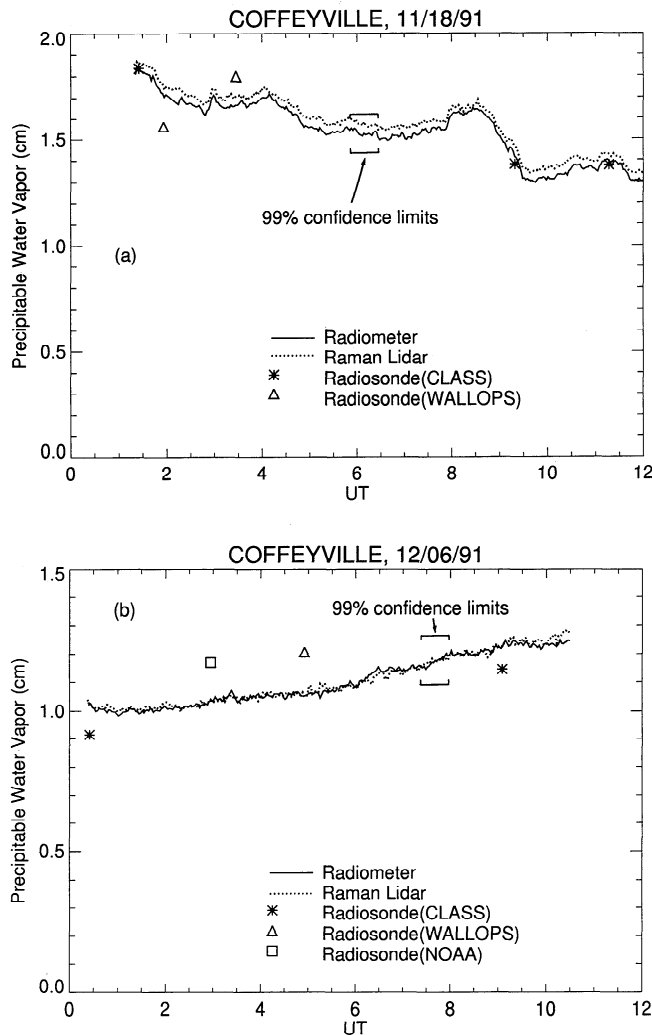


Figure 3. Time series of precipitable water vapor from the radiometer, Raman lidar, and radiosonde on (a) November 18, 1991, and (b) December 6, 1991.

rawinsonde measurements, with the best agreement being with the CLASS radiosondes. We show scatterplots of the total data set in Figure 4. The rms difference of 0.03 cm should be compared with the values of 0.17 cm reported by *Hogg et al.* [1983] and the more recent values of 0.11 cm of *Martner et al.* [1993]. The much better agreement between Raman and radiometer arises from at least four reasons: (1) the remote sensors are both simultaneously viewing the same zenith direction, although with different beamwidths (Raman beamwidth = 0.5×0.7 mrad, microwave beamwidths $\approx 2.5^\circ$); (2) these data are confined to clear-sky conditions, and the radiometer retrieval coefficients are determined for these conditions; (3) three rather than two channels were used in the radiometric retrievals; and (4) a nondiagonal experimentally determined covariance matrix S_e was used in the construction of retrieval coefficients. For comparison, using a dual-channel radiometer, *England et al.* [1992] achieved rms errors of from 0.02 to 0.08 cm.

As mentioned in section 3, the error in estimating water vapor from the surface to the first Raman range gate will also give an error in the comparisons of V . However, the microwave determinations of V do not use surface data. For

example, a typically observed error in absolute humidity of 0.5 g/m^3 in the first 200 m will give rise to an error in V of 0.01 cm, which is about 33% of the Raman-radiometer difference shown in Figure 3. In addition, if one would completely neglect the water vapor above 8.5 km, about 0.05 cm of error would occur; since we extrapolate the upper altitude water vapor, we estimate that the error from this source is less than 0.01 cm.

We also compared power spectra of V as determined by the two remote measurements and for the time periods shown in Figure 3. For the 3 hours of data, taken with 2-min averaging times, the Nyquist frequency was 15 cycles/h. For the computation of spectra, we used a spectral-windowing method that uses the spectral window of Parzen [*Jenkins and Watts, 1969*] with a maximum lag of 44 min. Typical examples of spectra are shown in Figure 5. For comparison we have plotted a line with a $-5/3$ slope that would represent, for a constant wind, the spectral decay of a single level of isotropic homogeneous turbulence. As would be expected from both the time series and the statistical results shown in Figures 3 and 4, the spectra are also in reasonable agreement.

5. Conclusion

The use of Raman lidar data for the detailed studies of tropospheric water vapor absorption and emission has significant potential. The vertical resolution of 75 m and the temporal resolution of 1 min have significant advantages over radiosondes which frequently are displaced from a radiometer's observing volume and which take about 30 min to traverse the major portion of the water vapor overburden. Another advantage is that the lidar can indicate the presence or absence of clouds, so that clear-sky radiative transfer calculations can be confidently made. On the negative side, the Raman soundings reach to ≈ 8.5 -km altitudes only during the night, and the lidar retrievals are normally limited to altitudes below cloud base.

We have examined three absorption models here. At the lower frequencies of 20.6 and 31.65 GHz and for the rela-

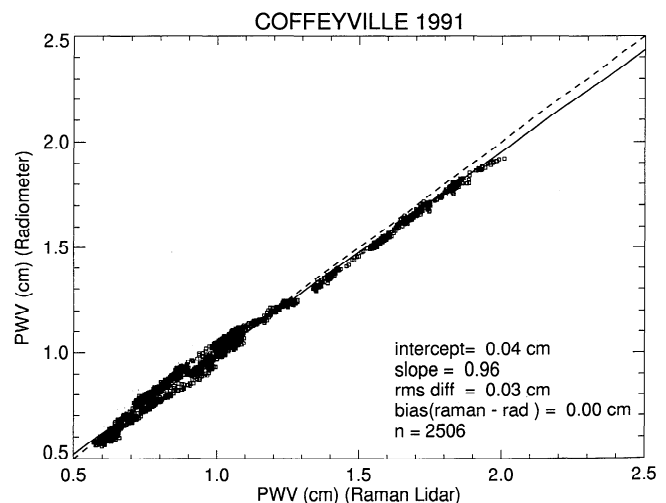


Figure 4. Comparison of radiometer-derived and Raman lidar measured precipitable water vapor. Dashed line is 45° and solid line is regression.

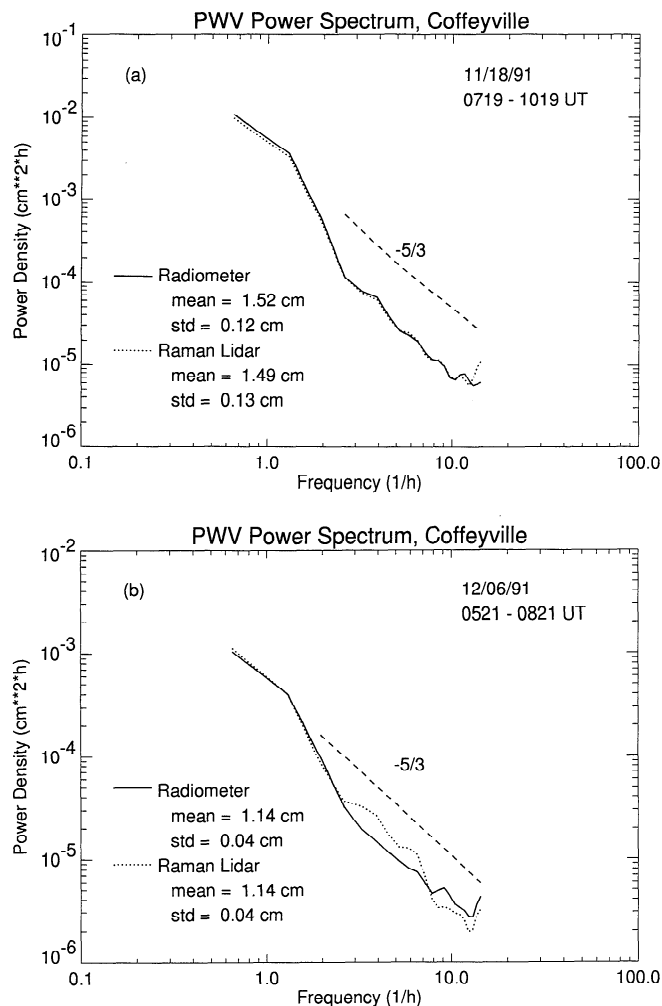


Figure 5. Examples of spectra of precipitable water vapor from the radiometer and the Raman lidar data taken on (a) November 18, 1991, and (b) December 6, 1991.

tively dry Coffeyville, Kansas, environment, the calculations based on RTE76 and RTE93 produced similar results, with rms differences between measurements and calculations of ≈ 0.5 K. However, the results at 90 GHz using RTE93 were not substantially better than the earlier RTE87 and may be worse. It was previously established that RTE76 poorly modeled 90-GHz emission. Since 90-GHz emission is not affected by changes in the 22.235 water vapor line parameters, the differences could be due to changes in the parameterization of the water vapor continuum or also in the description of the O_2 far wing behavior. Definitive experiments using collocated Raman lidar and microwave radiometers could be conducted in humid locations to address these issues.

The excellent temporal correlations between the Raman lidar's and the microwave radiometer's determination of precipitable water vapor confirms the ability of both of the instruments to follow rapid changes in moisture. The already demonstrated agreement in profile determination between the Raman lidar and the radiosondes lends further confirmation to the lidars ability as a meteorological research tool.

The ability to calculate downward radiances in spectral regions of low atmospheric transmission is also important for

the microwave remote sensing of moisture from satellites [Alishouse *et al.*, 1990a, b], since the downward flowing atmospheric radiance closely approximates the upward flowing atmospheric radiance. Although satellite retrievals of moisture and cloud liquid are also affected by variations in surface emissivity, better atmospheric absorption models are still fundamental to improved satellite retrievals. In addition, satellite flights over suitably located Raman lidar and microwave radiometers could prove very useful for improvements in satellite data validation and product improvement. For example, if these upward looking microwave radiometers had frequencies that coincided with, say, DMSP/SSM/I channels, a rich variety of data sets could be obtained.

Acknowledgments. The authors thank H. J. Liebe for providing us with copies of his latest MPM software as well as discussing several aspects of his work. The authors also thank R. G. Strauch, K. Moran, and D. Wertz for providing their interpolated RASS and rawinsonde data. The authors acknowledge R. Hill and B. Stankov for helpful comments on the manuscript. This work was partially supported by the Department of Energy's Atmospheric Radiation Measurements Program. R.A.F. is under contract at NASA Goddard Space Flight Center, Greenbelt, Maryland.

References

- Alishouse, J. C., S. A. Snyder, J. Vongsathorn, and R. R. Ferraro, Determination of oceanic total precipitable water from the SSM/I, *IEEE Trans. Geosci. Remote Sens.*, 28, 811–816, 1990a.
- Alishouse, J. C., J. B. Snider, E. R. Westwater, C. Swift, C. Ruff, S. Snyder, J. Vongsathorn, and R. R. Ferraro, Determination of cloud liquid water content using the SSM/I, *IEEE Trans. Geosci. Remote Sens.*, 28, 817–822, 1990b.
- Decker, M. T., and J. A. Schroeder, Calibration of ground-based microwave radiometers for atmospheric remote sensing, *NOAA Tech. Memo., ERL WPL-197*, 16 pp., Natl. Oceanic and Atmos. Adm., Washington, D. C., 1991.
- Elliott, W. P., and D. J. Gaffen, On the utility of radiosonde humidity archives for climate studies, *Bull. Am. Meteorol. Soc.*, 72, 1507–1520, 1991.
- England, M. N., R. A. Ferraro, S. H. Melfi, D. N. Whiteman, and T. A. Clark, Atmospheric water vapor measurements: Comparison of microwave radiometry and lidar, *J. Geophys. Res.*, 97, 899–916, 1992.
- England, M. N., F. J. Schmidlin, and J. M. Johansson, Atmospheric moisture measurements: A microwave radiometer-radiosonde comparison, *IEEE Trans. Geosci. Remote Sens.*, 31, 389–398, 1993.
- Ferraro, R. A., S. H. Melfi, D. N. Whiteman, and K. D. Evans, Raman lidar measurements of Pinatubo aerosols over southeastern Kansas during November–December 1991, *Geophys. Res. Lett.*, 19, 1599–1602, 1992.
- Fleming, H. E., N. C. Grody, and E. J. Katz, The forward problem and corrections for the SSM/T satellite microwave temperature sounder, *IEEE Trans. Geosci. Remote Sens.*, 29, 571–583, 1991.
- Garand, L., C. Grassotti, J. Halle, and G. Klein, On differences in radiosonde humidity-reporting practices and their implications for numerical weather prediction and remote sensing, *Bull. Am. Meteorol. Soc.*, 73, 1417–1423, 1992.
- Hogg, D. C., F. O. Guiraud, J. B. Snider, M. T. Decker, and E. R. Westwater, A steerable dual-channel microwave radiometer for measurement of water vapor and liquid in the troposphere, *J. Appl. Meteorol.*, 22, 789–806, 1983.
- Jenkins, G. M., and D. G. Watts, *Spectral Analysis and Its Applications*, 525 pp., Holden-Day, Oakland, Calif., 1969.
- Liebe, H. J., MPM—An atmospheric millimeter wave propagation model, *Int. J. Infrared Millimeter Waves*, 10, 631–650, 1989.
- Liebe, H. J., and D. H. Layton, Millimeter wave properties of the atmosphere: Laboratory studies and propagation modeling, *NTIA Rep. 87-24*, 74 pp., Natl. Tele. Inf. Adm., Boulder, Colo., 1987.
- Liebe, H. J., P. W. Rosenkranz, and G. A. Hufford, Atmospheric

- 60-GHz oxygen spectrum: New laboratory measurements and line parameters, *J. Quant. Spectrosc. Radiat. Transfer*, **48**, 629–643, 1992.
- Liebe, H. J., G. A. Hufford, and M. G. Cotton, Propagation modeling of moist air and suspended water/ice particles below 1000 GHz, paper presented at the AGARD Fifty-Second Special Meeting of the Panel on Electromagnetic Wave Propagation, pp. 3-1–3-10, *Advis. Group Aerosp. Res. Dev., Palma de Mallorca, Spain, May 17–21, 1993*.
- Martner, B. E., D. B. Wuertz, B. B. Stankov, R. G. Strauch, E. R. Westwater, K. S. Gage, W. L. Ecklund, C. L. Martin, and W. F. Dabberdt, An evaluation of wind profiler, RASS, and microwave radiometer performance, *Bull. Am. Meteorol. Soc.*, **74**, 599–616, 1993.
- May, P. T., R. G. Strauch, and K. P. Moran, The altitude coverage of temperature measurements using RASS with wind profiler radars, *Geophys. Res. Lett.*, **15**, 1381–1384, 1988.
- Melfi, S. H., and D. N. Whiteman, Observation of lower atmospheric moisture structure and its evolution using a Raman lidar, *Bull. Am. Meteor. Soc.*, **66**, 1288–1292, 1985.
- Melfi, S. H., D. Whiteman, and R. A. Ferrare, Observation of atmospheric fronts using Raman lidar moisture measurements, *J. Clim. Appl. Meteorol.*, **28**, 789–806, 1989.
- Rao, P. K., S. J. Holmes, R. K. Anderson, J. S. Winston, and P. E. Lehr, *Weather Satellites: Systems, Data, and Environmental Applications*, 503 pp., American Meteorological Society, Boston, Mass., 1990.
- Rosenkranz, P. W., Interference coefficients for overlapping oxygen lines in air, *J. Quant. Spectrosc. Radiat. Transfer*, **39**, 287–297, 1988.
- Schroeder, J. S., and E. R. Westwater, Users guide to WPL microwave radiative transfer software, *NOAA Tech. Memo. ERL WPL-213*, 84 pp., Natl. Oceanic and Atmos. Adm., Washington, D. C., 1991.
- Soden, B. J., S. A. Ackerman, D. O. C. Starr, S. H. Melfi, and R. A. Ferrare, Comparison of upper tropospheric water vapor from GOES, Raman lidar, and CLASS measurements during FIRE Cirrus 2, *J. Geophys. Res.*, in press, 1994.
- Wade, C. G., and D. E. Wolfe, Performance of the VIZ carbon hygrometer in a dry environment, in *Preprints, 12th Conference on Weather Analysis and Forecasting*, p. 58, American Meteorological Society, Boston, Mass., 1989.
- Waters, J. W., Absorption and emission of microwave radiation by atmospheric gases, in *Methods of Experimental Physics*, vol. 12B, edited by M. L. Meeks, *Radio Astron., Sect. 2.3*, 1976.
- Westwater, E. R., Ground-based remote sensing of meteorological variables, in *Atmospheric Remote Sensing by Microwave Radiometry*, edited by M. A. Janssen, pp. 145–213, John Wiley, New York, 1993.
- Westwater, E. R., M. J. Falls, and I. A. Popa Fotino, Ground-based microwave radiometric observations of precipitable water vapor: A comparison with ground-truth from two radiosonde observing systems, *J. Atmos. Oceanic Technol.*, **6**, 724–730, 1989.
- Westwater, E. R., J. B. Snider, and M. J. Falls, Ground-based radiometric observations of atmospheric emission and attenuation at 20.6, 31.65, and 90 GHz: A comparison of measurements and theory, *IEEE Trans. Antennas Propag.*, **AP-38**, 1569–1580, 1990.
- Whiteman, D. N., et al., Advanced Raman water vapor lidar, 16th International Laser Radar Conference, *NASA Conf. Publ. 3158*, part 2, pp. 483–484, 1992a.
- Whiteman, D. N., S. H. Melfi, and R. A. Ferrare, Raman lidar system for the measurement of water vapor and aerosols in the Earth's atmosphere, *Appl. Opt.*, **31**, 3068–3082, 1992b.
- Wilkinson, D. T., Anisotropy of the cosmic blackbody radiation, *Science*, **232**, 1517–1522, 1986.
- R. A. Ferrare, Hughes STX Corporation, Lanham, MD 20706.
 Y. Han (NRC Resident Assoc.), J. B. Snider, and E. R. Westwater, NOAA/ERL/ETL, 325 Broadway, Boulder, CO 80303.
 S. H. Melfi, Laboratory for Atmospheres, NASA GSFC, Greenbelt, MD 20771.

(Received February 15, 1994; revised May 13, 1994; accepted May 18, 1994.)